Effects of surgical joint destabilization on load sharing between ligamentous structures in the thoracic spine: A Finite Element investigation

Authors:

J. P. Little, PhD and C. J. Adam, PhD

Affiliations:

Paediatric Spine Research Group, Institute of Health and Biomedical Innovation, Queensland University of Technology, Brisbane, Australia

Corresponding Author:

Dr J P Little

Room O708, Level 7, O Block

Gardens Point Campus

Queensland University of Technology

2 George Street

Brisbane QLD 4000

Australia

Phone: +61 7 31385112

Email: j2.little@qut.edu.au

Financial Support:

1 Abstract

Background: In vitro investigations have demonstrated the importance of the ribcage in stabilising the thoracic spine. Surgical alterations of the ribcage may change load-sharing patterns in the thoracic spine. Computer models are used in this study to explore the effect of surgical disruption of the rib-vertebrae connections on ligament load-sharing in the thoracic spine.

Methods: A finite element model of a T7-8 motion segment, including the T8 rib, was developed using CT-derived spinal anatomy for the Visible Woman. Both the intact motion segment and the motion segment with four successive stages of destabilization (discectomy and removal of right costovertebral joint, right costotransverse joint and left costovertebral joint) were analysed for a 2000Nmm moment in flexion/extension, lateral bending and axial rotation. Joint rotational moments were compared with existing *in vitro* data and a detailed investigation of the load sharing between the posterior ligaments carried out.

Findings: The simulated motion segment demonstrated acceptable agreement with *in vitro* data at all stages of destabilization. Under lateral bending and axial rotation, the costovertebral joints were of critical importance in resisting applied moments. In comparison to the intact joint, anterior destabilization increases the total moment contributed by the posterior ligaments.

Interpretation: Surgical removal of the costovertebral joints may lead to excessive rotational motion in a spinal joint, increasing the risk of overload and damage to the remaining ligaments. The findings of this study are particularly relevant for surgical procedures involving rib head resection, such as some techniques for scoliosis deformity correction.

1.1 Key words

thoracic spine, costovertebral joints, ribcage, scoliosis biomechanics, finite element model, spinal ligaments

63

64

2 Introduction

The ribcage plays an important load bearing role in the functional behaviour of the thoracolumbar spine, providing between 31% and 40% of thoracic spine stiffness (Watkins IV *et al.*, 2005). Destabilizing the thoracic spine by removal of the intervertebral discs and rib-vertebrae connections significantly increases the rotational range of motion (ROM) of the motion segments (Oda *et al.*, 2002, Oda *et al.*, 1996) of the thoracic spine (Feiertag *et al.*, 1995).

While these *in vitro* studies provide insight into how the rib-vertebrae connections influence the biomechanics of the spine, they do not provide insight into how surgical alteration of these structures affects the load sharing in the remaining soft tissue structures, particularly the posterior ligaments. This is relevant firstly, in elucidating how individual structural elements (osseous anatomy, ligamentous structures, arthrodial joints, intervertebral discs) within the thoracic spinal joints contribute to resisting applied loads and secondly, in better understanding the change in biomechanics following surgical procedures involving disruption of the costovertebral and/or costotransverse joints, such as spinal deformity surgery for scoliosis. Computer models of the spine have been previously employed to investigate the mechanics of the intact and surgically altered spine, to assist in better understanding spine biomechanics in scoliosis patients. Computational analysis allows in-depth investigation of the mechanics of both intact and surgically altered joint structures; however, computer models must first be validated against in vitro experimental data. However, existing finite element (FE) models of the thoracolumbar spine either neglect to include a representation for the ribcage (Aubin *et al.*, 2003, Dumas *et al.*, 2005, Viviani *et al.*, 1986) or if the ribcage has been modelled, the rib-vertebrae connections are often highly simplified in their representation (Andriacchi *et al.*, 1974, Descrimes *et al.*, 1995, Gréalou *et al.*, 2002, Lee *et al.*, 1995, Sham *et al.*, 2005, Stokes and Laible, 1990). Moreover, these studies provide little detail to establish the accuracy of the ribcage representations employed, with validation of the modelling methodology based on comparisons of whole spine rotations with *in vitro* data

(Sham *et al.*, 2005). Of particular interest is the accurate simulation of the rib-vertebrae connections - the costovertebral and costotransverse joints - since these are the primary means of load transmission from the spine to the ribcage .

In the current study, an FE model of the T7-8 thoracic motion segment, including T8 ribs, was validated using *in vitro* data for relative changes in joint range of motion between an intact motion segment and four stages of surgical joint destabilization (Oda *et al.*, 2002). Following this, an in-depth investigation of the load sharing between the posterior ligaments spanning the motion segment was performed.

3 Materials and Methods

An FE model of an adult, osseo-ligamentous, T7-8 thoracic spinal motion segment (SMS), including the T8 left and right ribs, was generated using anatomy from the Visible Woman computed tomography (CT) dataset (The Visible Human Project, US National Library of Medicine). Five separate model cases were analyzed; an intact SMS, and four successive stages of anterior joint destabilization investigated *in vitro* by Oda *et al*. (Oda *et al.*, 2002). Comparison of FE model predictions with the experimental data presented by Oda *et al*. (Oda *et al.*, 2002) enabled validation of the model. Following model validation, relative changes in ligament loads at each stage of destabilization were simulated, to investigate the mechanical influence of spinal joint structures on SMS biomechanics. While the thoracic spine segments tested by Oda *et al*. (Oda *et al.*, 2002) included both ligamentous and muscular structures, without muscle activation it is expected that the spinal ligaments would primarily control the passive joint kinematics, therefore no attempt was made to include muscles in the model. Moreover, the stiffness of the spinal muscles are up to three orders of magnitude lower than ligament stiffnesses (Lu *et al.*, 1996, Ward *et al.*, 2009), therefore their contribution to passive joint biomechanics would be minimal.

3.1 Intact T7-8 SMS – Geometry and FE Model Details

Our technique for deriving FE models from CT scan data of the thoracolumbar spine and ribcage has been previously described (Little and Adam, 2009, Little *et al.*, 2008) and will not be included herein. These techniques were used to create an FE model of the T7 and T8 vertebrae and T8 left and right ribs. To replicate the anatomy of the motion segments tested by Oda *et al*. (Oda *et al.*, 2002), only the posterior 5cm of the left and right rib was simulated. For the sake of brevity, references to the T7-8 SMS will assume this segment includes the T8 left and right ribs. Details of element types used to represent the components of the SMS are listed in Table 1. The meshed SMS is shown in Figure 1. The left and right costo-transverse joints (CTJt) were represented as rigid, kinematic constraints between the lateral-most point on the transverse processes of T8 and the adjacent region of the ribs. Mesh sensitivity analysis off the 4-node shell elements representing the ribs found that doubling mesh density changed the predicted joint stiffness by less than 2%.

3.2 Costovertebral Joint – Anatomy and Simulation

Anatomically, the costo-vertebral joints (CVJt) are arthrodial joints, with articulating surfaces on the medial rib and superior/inferior postero-lateral cortices of the adjoining vertebrae. Strong ligaments span the joint, both in the form of the surrounding joint ‘capsule’ as well as intra-joint ligamentous connections, with the radiate and interarticular ligament connecting the rib directly to both vertebrae and the lateral surface of the intervertebral disc (Gray, 1918). Given the biomechanical importance of these joints (Oda *et al.*, 2002, Watkins IV *et al.*, 2005), it was necessary to simulate the CVJts in detail in the current study so as to accurately model their structure and function.

In the current study, the complex articulation between rib heads and the adjacent vertebrae and intervertebral discs was represented using ‘clusters’ of beams, connecting the medial end of the T8 ribs and the T7/T8 vertebrae and intervertebral disc surfaces, as shown in Figure 1B. The cross-sectional area of the CVJt was estimated to be 46mm^2, based on the dimensions of the adjacent vertebrae and this area was evenly subdivided between each beam cross-

section. To our knowledge, the present study presents the first validation of a thoracic SMS FE model incorporating a detailed representation for the CVJt articulations.

3.3 Materials

The material representations employed for all model components, except the vertebra-rib connections, have been described previously (Little and Adam, 2009). The material parameters employed for these components are listed in Table 1. All ligaments were simulated as tension-only, axial connectors joining the relevant bony attachment points on the T7 and T8 vertebrae. No ligament wrapping was simulated. The ligaments were represented using piece-wise, nonlinear, elastic behaviour and nonlinear stiffness data were derived from existing literature (Chazal *et al.*, 1985, Nolte *et al.*, 1990, Shirazi-Adl *et al.*, 1986), using ligament connector lengths derived from the bony anatomy of the Visible Woman T7/8 vertebral joint. Ligament cross-sectional areas were derived from Chazal *et al.* (Chazal *et al.*, 1985) and Lu *et al.* (Lu *et al.*, 1996).

In the current study, bending and torsional properties for the simulated CVJts were derived from the bending and torsional stiffnesses presented by Lemosse *et al*. (Lemosse *et al.*, 1998), following costo-transverse joint dissection (Table 1). The experimental stiffnesses (Lemosse *et al.*, 1998) were averaged for the positive and negative loading directions. An approximated total CVJt area of 46mm^2 (including the rib connection to both vertebrae and the intervertebral disc) was subdivided between each beam element representing the CVJt (Figure 1B). Beam elements representing the CVJts were assigned compressive stiffness values derived from Andriacchi *et al*. (Andriacchi *et al.*, 1974) (Table 1).

3.4 Simulated destabilization of the SMS

Following analysis of the intact T7/8 SMS, four successive stages of ‘anterior destabilization’ were simulated in the current study, to replicate the anterior destabilization steps carried out by Oda *et al*. (Oda *et al.*, 2002). These included:

i. Discectomy

ii. Removal of the right CVJt

iii. Removal of the right CTJt

iv. Removal of the left CVJt

The intact SMS FE model will be referred to as *intact*.

3.4.1 Stage i - Discectomy

All meshed components of the simulated intervertebral disc, including the anulus fibrosus brick elements, collagen fibre tension-only connectors and hydrostatic fluid elements were removed (Figure 2A, highlighted with ▨). The connector elements representing the ALL and PLL were removed from the anterior and posterior margins of the T7/T8 disc space. Finally, beam elements connecting the mid-height, medial rib and the lateral intervertebral disc in the CVJts were removed, leaving only the elements linking the ribs with the T7 and T8 vertebral cortices (Figure 2A, highlighted with ▨). This model will be referred to as *discectomy*.

3.4.2 Stage ii – Removal of the right Costo-vertebral joint

The remaining CVJt beam elements connecting the right rib head to the T7 and T8 vertebral cortices were removed from the *discectomy* model. This model will be referred to as *RtCVJt* (Figure 2A, highlighted with ▨).

3.4.3 Stage iii – Removal of right Costo-transverse joint

The linear, kinematic constraints that simulated the right CTJt were removed from the *RtCVJt* model. These constraints were connecting the right T8 transverse process to the adjacent region of the right rib (Figure 2A, highlighted with ▨). This model will be referred to as *RtCTJt*. Following this stage of destabilization, the right rib was no longer connected to the vertebra-disc-vertebra segment and as such, did not contribute to the mechanics of the analyzed motion segment.

3.4.4 Stage iv – Removal of the left Costo-vertebral joint

Finally, the remaining beam elements spanning the left CVJt were removed (Figure 2B, highlighted with) – these included beams connecting the left rib to the T7 and T8 vertebral cortices. This model will be referred to as *LftCVJt* (Figure 2C). Following this stage of destabilization, only the left CTJt connected the vertebra-disc-vertebra segment to the left rib.

3.5 Loading and Boundary Conditions

Three different load cases were applied to each of the five models, to replicate the loading and boundary conditions investigated by Oda *et al*. (Oda *et al.*, 2002), who applied 2000Nmm moment loading about fixed axes to investigate the response of the cadaveric SMS to flexion-extension, left and right lateral bending and axial rotation. The 2000Nmm moment used results in a physiological range of motion for a T7/8 spinal joint (Mannion *et al.*, 2004). The antero-lateral rib ends were not constrained in the models, as was the case for the cadaveric joints tested experimentally.

In the current study, the lower T8 endplate was rigidly constrained in all degrees-of-freedom to a node at the centroid of the T8 vertebral body. A rigid, kinematic constraint was simulated on the upper T7 endplate, constraining the motion of this surface to a loading point at the centre of the intervertebral disc, corresponding to the 'midcolumn' axis of rotation used by Oda (Oda et al, 2002). A ±2000Nmm moment applied at this point simulated flexion-extension, left-right lateral bending and left-right axial rotation, and all other degrees of freedom of the loading point were constrained following Oda *et al*. (Oda *et al.*, 2002).

3.6 Analyses

Analyses were performed on an SGI Altix 4700 supercomputer (96x64bit processors, 198 GB RAM) using Abaqus/Standard 6.7.1 (Simulia, Providence, RI). All analyses were quasi-static with non-linear (finite strain) geometry capability enabled.

3.6.1 SMS Model validation

Oda *et al*. (Oda *et al.*, 2002) presented data for the percentage change in joint ROM after each stage of destabilization, relative to the intact joint (ie only relative changes were given, not absolute values). To validate the FE model, simulated absolute rotations of the *intact* model were compared with *in vitro* data from an earlier study (Panjabi *et al.*, 1976), detailing the response of a T7-8 thoracic motion segment to an applied moment of ±2000Nmm about the three axes of motion. Following this, the expected *in vitro* ROM at each stage of destabilization was calculated using the data for relative increases in rotation presented by Oda *et al*. (Oda *et al.*, 2002) and the intact ROM presented by Panjabi *et al*. (Panjabi *et al.*, 1976). These data were expressed as joint stiffness for both the *in vitro* and simulated SMS, with stiffness (Nmm.degree^{-1}) calculated using the applied moment (2000Nmm) and the angular ROM.

3.6.2 Reaction Forces at the Loading Point and Reaction Moment at the Point of Constraint

Oda *et al.* (Oda *et al.*, 2002) stated that the loading conditions applied experimentally permitted constrained motion about one degree-of-freedom. These loading conditions were reproduced in the current study. However, this is a non-physiological loading state, since physiological joint motion occurs about a 'centrode of motion' (Pearcy and Bogduk, 1988). Therefore constraining the point of loading to reproduce this *in vitro* loading condition generated reaction forces at this point. These reaction forces were investigated as were the reaction moments at the point of constraint for each analysis. These reaction moments were the sum of the applied moment (2000Nmm) and the moment resulting from the reaction forces generated at the point of loading (Figure 4).

3.6.3 Investigation of SMS Mechanics

Following this, a detailed investigation of the load sharing between the five posterior ligaments – inter-transverse, supra-/inter-spinous, ligamentum flavum and capsular ligaments – was carried out for the *intact* model and at each stage of destabilization. The resistive moment provided by each ligament about the point of loading was expressed as a percentage of the applied 2000Nmm

moment. The ligament resistive moment was calculated using the maximum connector force in elements simulating these ligaments and the normal distance between the centre of the disc (moment application point) and the centre of the ligament connector. The anterior and posterior longitudinal ligaments were not included in this comparison, since they were removed at the first stage of joint destabilization.

Total ligament moment, TLM, was calculated as the total of the percentages of resistive moment carried by the posterior ligaments, so a TLM value of 100±0.5% (solution accuracy $5x10^{-3}$) implied the ligaments alone were responsible for resisting the applied moment. TLM<100% implied that the remainder of the applied moment was carried by anterior structures, namely the ALL, PLL and intervertebral disc.

4 Results

4.1 SMS Model Validation

Figure 3 compares *in vitro* and FE model results for the intact model and the four levels of joint dissection under the three loading directions. The average error between simulated and *in vitro* stiffness was 31%, 13% and 7% for flexion-extension, lateral bending and axial rotation, respectively, for all five models. While the errors in simulated joint stiffness were generally low, the exception was for the *intact* and *LftCVJt* models under lateral bending and the *LftCVJt* model under flexion-extension (Figure 3 A, B). These results demonstrated differences in stiffness of 42%, -54% and 59%, respectively – this negative difference indicating the simulated SMS after the last stage of destabilization was overly lax in comparison to the *in vitro* stiffness derived from Oda *et al*. (Oda *et al.*, 2002) and Panjabi *et al* (Panjabi *et al.*, 1976). Overall, the simulated SMS tended to overestimate rather than underestimate joint stiffness and the average error in simulated stiffness for all models, under the three load cases, was 17%.

4.2 Reaction Forces and Moments

The reaction forces at the point of loading ranged from 0.3N to 120N (Table 2) and resulted in a total resistive moment at the point of constraint in T8 which was generally greater than the applied 2000Nmm moment (Tables 3, 4 and 5). In some analyses; however, the resistive moment was less than the applied 2000Nmm moment - this occurred for the flexion-extension and axial rotation load cases (Figure 4).

4.3 Investigation of SMS Mechanics

The predicted proportions of TAM resisted by each of the posterior ligaments, and how these proportions change with successive dissection of the joint are shown in Tables 3, 4 and 5. The simulated ROM in all five models was subdivided according to positive or negative rotation about the three axes, thus highlighting asymmetries in load-sharing during bi-directional loading.

Under all three motions there was no change in the SMS rotation following removal of the right CTJt. For a 2000Nmm applied moment, the supra-/inter-spinous ligament provided no resistance to motion about all three axes. The imbalance in the contralateral ligament moments for all except the supra-/inter-spinous ligament, is indicative of the inherent, anatomical asymmetry in the human spinal motion segments.

The posterior ligaments, the left CTJt and the zygapophyseal joints were the only structures that remained spanning the spinal joint in the *LftCVJt* model. Under extension, left lateral bending and right/left axial rotation, the TLM observed for these models suggested that structures other than the ligaments were contributing to resisting the applied moment .The results of these analyses showed contact pressures generated on the zygapophyseal joint surfaces and the comparatively high values for moment resisted by the capsular ligaments suggested that the contact forces transmitted across the zygapophyseal joints were providing a greater contribution to resisting the TLM than the left CTJt.

4.3.1 Flexion-Extension

In the *intact* model, the posterior ligaments provide no resistance to the applied moment during extension. With successive destabilization of the joint, the capsular ligaments are the only ligaments which resist the applied moment, and there was a 31% increase in TLM with removal of the right CVJt and a further 53% increase with removal of the left CVJt.

Under flexion loading, the resistive moment is primarily provided by the inter-transverse ligament and ligamentum flavum, until both CVJts are removed. In the *RtCTJt* model, over 40% of the applied moment is resisted by the remaining left CVJt. Load sharing in the *LftCVJt* model demonstrated that the capsular ligaments were resisting 35% of the applied moment.

4.3.2 Left and Right Lateral Bending

In the *intact* model, left and right lateral bending is primarily resisted by structures other than the posterior ligaments and this is true until both the left and right CVJts are removed. Removal of the left CVJt increases the portion of moment resisted by the ligaments, from 8.4 and 7.5% to 99.9 and 99.3% for right and left lateral bending, respectively.

4.3.3 Left and Right Axial Rotation

In both the *intact* and *discectomy* models, the posterior ligaments provide less than 1% of the total resistive moment under axial rotation. Removal of the right CVJt increases the TLM to 3.2% (left) and 4.4% (right) and removal of the left CVJt increases the TLM further to 98.4 (left) and 98.3% (right). In the *LftCVJt* model, the capsular ligaments are responsible for resisting the majority of the applied moment. The ROM in the *LftCVJt* model is approximately 1.3 times the ROM in the *RtCTJt* model and 5.6 times the ROM of the *intact* model.

5 Discussion

The current study presents a detailed finite element study of the mechanics of the T7-8 motion segment including the T8 ribs, validated by comparison with previous *in vitro* data. Following validation of the model predictions by comparison with previous experiments, the effect of surgical dissection on load

sharing between posterior ligaments, rib-vertebrae connections, and soft tissues spanning the joint space (ALL, PLL, intervertebral disc) was investigated. Ideally, a computer model such as the one used in this study would be validated by conducting both an experimental and a computational investigation of spinal joint biomechanics using the same joint anatomy. This was not possible in the current study, since the best available experimental data for rib-vertebra destabilization on human subjects is that of a previous study (Oda *et al.*, 2002). We suggest that given the uncertainties in anatomy between model and experiment, the predicted trends in joint stiffness with successive destabilization (Figure 3) capture the experimentally measured trends well for all three directions of loading.

A qualitative comparison of the change in stiffness between the *intact* model and after the four stages of destabilization, suggested that the relative influence of each removed structure on the overall joint ROM was similar between the simulated and *in vitro* SMS. The relatively low average error (<20%) between the simulated and *in vitro* stiffness suggested the detailed modeling approach we have employed to represent the rib-vertebra connections provides a valid representation of the mechanics of the thoracic motion segment. The *in vitro* data presented by Panjabi *et al.* (Panjabi *et al.*, 1976) was for an experimental loading which applied unconstrained torsional moments about the three axes of motion. Conversely, the testing procedure used by Oda *et al* (Oda *et al.*, 2002) and simulated in the current study applied constrained torsional moments on the SMS, with only one degree of freedom. This difference in experimental constraints between Oda *et al.* (Oda *et al.*, 2002) and Panjabi *et al.* (Panjabi *et al.*, 1976) potentially explains the marginally stiffer predicted response for the *intact* model compared to the experimental data from Panjabi *et al.* (Panjabi *et al.*, 1976).

Previous full spine FE models including the ribs have used relatively simple representations for the CVJts, representing these joints variously using a single, tension-only (Sham *et al.*, 2005) or bilinear spring (Andriacchi *et al.*, 1974), a ball-and-socket joint (Descrimes *et al.*, 1995, Stokes and Laible, 1990) or a single, linear, beam element (Gréalou *et al.*, 2002, Lee *et al.*, 1995). These

representations do not include the anatomical connection between the rib head and intervertebral disc. Material parameters for these linear connections have previously been derived using *in vitro* mechanical data from experimental testing of full spines (Sham *et al.*, 2005). This approach does not account for the complex load sharing relationship between the ribs, vertebrae and intervertebral discs. The CVJt representation used in the current study addressed these limitations in previous studies, by simulating the connection between the rib head and adjacent intervertebral disc and vertebrae and deriving material properties for the joints from detailed experimental studies of the CVJt bending properties (Lemosse *et al.*, 1998).

In order for displacement controlled loading conditions to reproduce the physiological motion of the SMS *in vitro*, the prescribed rotational motion should be applied about a 'centrode of motion' (Pearcy and Bogduk, 1988). This is a locus comprising the instantaneous centre of rotation (the point about which pure rotational motion occurs) of the joint for each phase of rotational motion about a particular axis (Pearcy and Bogduk, 1988). However, Oda *et al*. (Oda *et al.*, 2002) defined one centre of rotation for all rotational motions – this location was reproduced in the current study. The predicted reaction forces generated at this point of loading suggested that, by constraining the degrees-of-freedom of the point about which rotational motion was prescribed, this loading method did not appropriately reproduce the physiological motion of a human SMS. If the point of loading was located at the physiological joint centroid, these forces would be zero. However, the experimental data provided by Oda *et al*. (Oda *et al.*, 2002) still provide useful information for model validation.

In the destabilized models, the observation that the simulated supra-/inter-spinous ligaments provided no resistance to the applied moment was in keeping with the *in vitro* findings of Hindle *et al*. (Hindle *et al.*, 1990), who observed that these structures provided minimal 'mechanical assistance' to the spinal joints for physiological flexion motions. Oda *et al*. (Oda *et al.*, 2002) found no significant change in the joint flexion-extension ROM following removal of the right CTJt; a trend also observed in the simulated SMS.

Results for lateral bending suggest that structures other than the posterior ligaments are responsible for resisting the applied moments in the intact and destabilized joint. While the presented results do not provide data on relative load sharing between the left and right CVJts in the *discectomy* model, the considerable increase in resistive moment carried by the ligaments when the left CVJt is removed, suggests that these joints preferentially carry the majority of the lateral bending moment in either an intact or discectomy-destabilized joint. Moreover, there was a four-fold increase in lateral bending ROM once the left CVJt was removed and the ROM in the *LftCVJt* model was 12-16 times greater than the *in vitro* ROM for the intact T7-8 joint (Panjabi *et al.*, 1976). These results suggest that compromising the mechanical integrity of the CVJts may have a detrimental influence on SMS joint mechanics under lateral bending, leading to hyper-motion in the joint. This is relevant to patients undergoing scoliosis corrective surgery involving removal of the rib-heads to better mobilize the spinal joint and achieve improved correction (Kaneda *et al.*, 1997). While these joints will subsequently be re-stabilized with rigid instrumentation, during the intra-operative physical manipulation and compression of the joint to achieve correction of the lateral deformity, there is a potential for the spinal ligaments to be overloaded.

The effect of surgical destabilization on thoracic joint stability is relevant to adolescent scoliosis surgery using anterior approaches. However, the costovertebral joints in adolescents are less ossified than in the adult spine (Gray, 1918), potentially making them more flexible than a mature joint. As such, inferences made from these computational results, relating to adolescent spinal deformity correction, must be interpreted in light of this limitation.

These model predictions highlight the changed biomechanical role of the ligaments in a spinal joint which has been destabilized due to discectomy and compromise/removal of the CVJts. Compressive joint forces in excess of 1kN have been measured intra-operatively (Cunningham *et al.*, 2009) during deformity correction surgery for scoliosis, which would equate to an applied lateral bending moment in the order of $1x10^4$Nmm at the spinal joint. Under such

high applied forces, without the stabilizing contribution of the rib-vertebra connections, there is a high likelihood that ligament forces/strains may exceed the relevant rupture values (Chazal *et al.*, 1985, Nolte *et al.*, 1990). In agreement with the current analyses, Feiertag *et al*. (Feiertag *et al.*, 1995) observed that discectomy and rib head resection resulted in a significant increase in the rotational ROM of thoracic joints. In the context of surgical deformity correction for scoliosis, they suggested this additional rotation in the destabilized condition could be indicative of an achievable correction following scoliosis surgery; that is, over and above the correction seen on bending films prior to surgery. Kaneda *et al*. (Kaneda *et al.*, 1997) concluded that rib head resection permitted a higher correction rate to be achieved by destabilizing the rigid thoracic scoliosis. .

6 Conclusion

Finite element computer models of the thoracic spine and ribcage have the potential to predict loads experienced in individual soft tissue structures during spinal motions. Overall, the costo-vertebral joints appear to be of critical importance to the mechanical function of the spinal motion segments. Surgically compromising the mechanical integrity of these joints will likely lead to soft tissue structures surrounding the osseous spinal anatomy resisting greater loads than in the intact/healthy joint, and may bring with it a risk of soft tissue overload and ligament damage.

7 Table Captions

Table 1:

Element representations and material parameters used for the T7-8 FE model. (CL = capsular ligament, ITV = inter-transverse ligament, SSP – combined supra/inter-spinous ligament, ALL = anterior longitudinal ligament, PLL = posterior longitudinal ligament, LF – ligamentum flavum)

Table 2:

Reaction force at the point of loading (Newtons) (RF1 – positive in the posterior direction; RF2 – positive in the right lateral direction; RF3 – positive in the superior direction)

Table 3:

Load sharing between posterior ligaments under flexion-extension loading. Flexion = negative rotation. (ITVL/R = intertransverse ligament, left and right; SSP = supra-/inter-spinous ligament; FLAVL/R = ligamentum flavum, left and right; CAPL/R = capsular ligament, left and right, TLM = total ligament moment)

Table 4:

Load sharing between posterior ligaments under left and right lateral bending. Right lateral bending = negative rotation. (ITVL/R = intertransverse ligament, left and right; SSP = supra-/inter-spinous ligament; FLAVL/R = ligamentum flavum, left and right; CAPL/R = capsular ligament, left and right, TLM = total ligament moment)

Table 5:

Load sharing between posterior ligaments under left and right axial rotation. Right axial rotation = negative rotation. (ITVL/R = intertransverse ligament, left and right; SSP = supra-/inter-spinous ligament; FLAVL/R = ligamentum flavum, left and right; CAPL/R = capsular ligament, left and right, TLM = total ligament moment)

8 Figure captions

Figure 1:

Finite element mesh for a T7/8 single motion segment with ribs (T8), viewed from the left antero-lateral direction. Yellow elements = intervertebral disc; Purple elements = CVJt; Green lines posteriorly = posterior bony structures (assumed rigid), Blue broken lines = posterior ligaments. A. Full SMS, B. showing CVJt beam connections from the left rib to the vertebrae and intervertebral disc.

Figure 2:

Four stages of SMS joint destabilization. Discectomy; Remove right CVJt; Remove right CTJt; Remove left CVJt. A, B. Four stages of destabilization; C Left postero-lateral view showing fully destabilized joint with only the left CTJt connecting the vertebra-disc-vertebra motion segment to the ribs – the right rib is shown for consistency but did not contribute to the joint mechanics.

Figure 3:

Comparison of *in vitro* and simulated joint stiffness, for an applied moment load of 2000Nmm about the three axes of motion, for the intact case and the four stages of joint destabilization . A. Flexion-extension; B. Left and right lateral bending; C. Left and right axial rotation.

Figure 4:

Schematic of the T7/8 SMS (viewed from the left lateral direction) for the flexion loadcase applied to the *LftCVJt* model, demonstrating an instance where the resistive moment at the point of constraint is less than the applied 2000Nmm moment. The schematic shows the applied flexion moment at the point of loading in the intervertebral disc; the reaction force components and resultant at this point; and the reaction moment at the fixed boundary constraint on T8.

9 Bibliography

Andriacchi, T., Schultz, A., Belytschko, T., Galante, J., 1974.A model for studies of mechanical interactions between the human spine and rib cage. J Biomech, 7, 497-507.

Aubin, C. E., Petit, Y., Stokes, I. A., Poulin, F., Gardner-Morse, M., Labelle, H., 2003.Biomechanical modeling of posterior instrumentation of the scoliotic spine. Comput Methods Biomech Biomed Engin, 6, 27-32.

Chazal, J., Tanguy, A., Bourges, M., Gaurel, G., Escande, G., Guillot, M., Vanneuville, G., 1985.Biomechanical properties of spinal ligaments and a histological study of the supraspinal ligament in traction. J Biomech, 18, 167-76.

Cunningham, H., Little, J. P., Adam, C. J. (2009) In *ACSR Annual Meeting*Adelaide, Australia.

Descrimes, J. L., Aubin, C. E., Boudreault, F., Skalli, W., Zeller, R., Dansereau, J., Lavaste, F., 1995. Modelling of facet joints in a global finite element model of the spine: Mechanical aspects, In: D'Amico, M., Merolli, A. and Santambrogio, C., (Ed,^(Eds), Three dimensional analysis of spinal deformities, IOS Press.

Dumas, R., Lafage, V., Lafon, Y., Steib, J. P., Mitton, D., Skalli, W., 2005.Finite element simulation of spinal deformities correction by in situ contouring technique. Comput Methods Biomech Biomed Engin, 8, 331-7.

Feiertag, M. A., Horton, W. C., Norman, J. T., Proctor, F. C., Hutton, W. C., 1995.The effect of different surgical releases on thoracic spinal motion. A cadaveric study. Spine, 20, 1604-11.

Gray, H. G. (1918) (Ed, Lewis, W. H.) Lea & Febiger.

Gréalou, L., Aubin, C. E., Labelle, H., 2002.Rib cage surgery for the treatment of scoliosis: A biomechanical study of correction mechanisms. J Orthop Res, 20, 1121-8.

Hay, D., Izatt, M. T., Adam, C. J., Labrom, R. D., Askin, G. N., 2008.The use of fulcrum bending radiographs in anterior thoracic scoliosis correction: A consecutive series of 90 patients. Spine, 33, 999-1005.

Hindle, R. J., Pearcy, M. J., Cross, A., 1990.Mechanical function of the human lumbar interspinous and supraspinous ligaments. J Biomed Eng, 12, 340-4.

Kaneda, K., Shono, Y., Satoh, S., Abumi, K., 1997.Anterior correction of thoracic scoliosis with kaneda anterior spinal system. A preliminary report. Spine, 22, 1358-68.

Lee, M., Kelly, D. W., Steven, G. P., 1995.A model of spine, ribcage and pelvic responses to a specific lumbar manipulative force in relaxed subjects. J Biomech, 28, 1403-8.

Lemosse, D., Le Rue, O., Diop, A., Skalli, W., Marec, P., Lavaste, F., 1998.Characterization of the mechanical behaviour parameters of the costo-vertebral joint. Eur Spine J, 7, 16-23.

Little, J. P., Adam, C. J., 2009.The effect of soft tissue properties on spinal flexibility in scoliosis: Biomechanical simulation of fulcrum bending. Spine, 34, E76-E82.

Little, J. P., De Visser, H., Pearcy, M. J., Adam, C. J., 2008.Are coupled rotations in the lumbar spine largely due to the osseo-ligamentous anatomy? - a modelling study. Computational Methods in Biomechanics and Biomedical Engineering, 11, 95-103.

Lu, Y. M., Hutton, W. C., Gharpuray, V. M., 1996.Do bending, twisting, and diurnal fluid changes in the disc affect the propensity to prolapse? A viscoelastic finite element model. Spine, 21, 2570-9.

Mannion, A. F., Knecht, K., Balaban, G., Dvorak, J., Grob, D., 2004.A new skin-surface device for measuring the curvature and global and segmental ranges of motion of the spine: Reliability of measurements and comparison with data reviewed from the literature. Eur Spine J, 13, 122-36.

Nolte, L. P., Panjabi, M., Oxland, T., 1990. Biomechanical properties of lumbar spinal ligaments, In: Heimke, G., Soltesz, U. and Lee, A. J. C., (Ed,^(Eds), Clinical implant materials, Elsevier Science Publishing, Amsterdam, pp. 663-668.

Oda, I., Abumi, K., Cunningham, B. W., Kaneda, K., McAfee, P. C., 2002.An in vitro human cadaveric study investigating the biomechanical properties of the thoracic spine. Spine, 27, E64-70.

Oda, I., Abumi, K., Lu, D., Shono, Y., Kaneda, K., 1996.Biomechanical role of the posterior elements, costovertebral joints, and rib cage in the stability of the thoracic spine. Spine, 21, 1423-9.

Panjabi, M. M., Brand, R. A., Jr., White, A. A., 3rd, 1976.Mechanical properties of the human thoracic spine as shown by three-dimensional load-displacement curves. J Bone Joint Surg Am, 58, 642-52.

Pearcy, M. J., Bogduk, N., 1988.Instantaneous axes of rotation of the lumbar intervertebral joints. Spine, 13, 1033-41.

Sham, M. L., Zander, T., Rohlmann, A., Bergmann, G., 2005.Effects of the rib cage on thoracic spine flexibility. Biomed. Technik, 50, 361-365.

Shirazi-Adl, A., Ahmed, A. M., Shrivastava, S. C., 1986.Mechanical response of a lumbar motion segment in axial torque alone and combined with compression. Spine, 11, 914-27.

Stokes, I. A., Laible, J. P., 1990.Three-dimensional osseo-ligamentous model of the thorax representing initiation of scoliosis by asymmetric growth. J Biomech, 23, 589-95.

Viviani, G. R., Ghista, D. N., Lozada, P. J., Subbaraj, K., Barnes, G., 1986.Biomechanical analysis and simulation of scoliosis surgical correction. Clin Orthop, 40-7.

Ward, S. R., Tomiya, A., Regev, G. J., Thacker, B. E., Benzl, R. C., Kim, C. W., Lieber, R. L., 2009.Passive mechanical properties of the lumbar multifidus muscle support its role as a stabilizer. J Biomech, 42, 1384-9.

Watkins IV, R., Watkins III, R., Williams, L., Ahlbrand, S., Garcia, R., Karamanian, A., Sharp, L., Vo, C., Hedman, T., 2005.Stability provided by the sternum and rib cage in the thoracic spine. Spine, 30, 1283-1286.

Table(s)

Table 1 Element representations and material parameters used for the T7-8 FE model. (CL = capsular ligament, ITV = inter-transverse ligament, SSP – combined supra/inter-spinous ligament, ALL = anterior longitudinal ligament, PLL = posterior longitudinal ligament, LF – ligamentum flavum)

	Element representation	*Material representation*	*Reference*
Cortical Bone	3D, 4-node shell	Linear elastic: E = 11,300 MPa ν = 0.2	Lu et al., 1996
Cancellous Bone	3D, 8-node, brick	Linear elastic: E = 140 MPa ν = 0.2	Lu et al., 1996
Intervertebral disc: Annulus ground matrix	3D, 8-node brick	Hyperelastic, Mooney-Rivlin: C_{10} = 0.7 C_{01} = 0.2	Little et al., 2007; Natali 1991
Collagen fibres	3D, tension-only link (rebar elements)	Linear elastic: E = 500MPa ν = 0.3	Kimpara et al., 2005; Kumaresan et al., 1999
Nucleus pulposus	3D, 4-node, hydrostatic fluid	Incompressible	Nachemson 1960
Posterior bony elements	3D, 2-node, rigid beams	Rigid	
Zygapophyseal joint surfaces	3D, 4-node, shell element	Cortical Bone: Linear elastic: E = 11,300 MPa ν = 0.2	
Costo-vertebral joint:	3D, 2-node beams	Linear elastic: E_{compr} = 245N.mm^{-1} Torsion stiffness, k = 4167 Nmm.rad^{-1} Bending stiffness, k = 6706 Nmm.rad^{-1} (average antero-posterior and cranio-caudal flexion stiffness)	Andriacchi et al., 1974; Lemosse et al., 1998

Ligaments	3D, 2-node, tension-only, connectors	Piecewise, non-linear	CL, SSP - Shirazi-Adl et al., 1986; ITV - Chazal et al., 1985; ALL, PLL, LF - Nolte et al., 1990

Table 2 Reaction force at the point of loading (Newtons) (RF1 – positive in the posterior direction; RF2 – positive in the right lateral direction; RF3 – positive in the superior direction)

		Flexion	Extension	Right Lateral Bending	Left Lateral Bending	Right Axial Rotation	Left Axial Rotation
Intact	**RF1**	**-18.2**	**0.3**	**-16.5**	**-14.5**	**-8.6**	**-15.6**
	RF2	**3.4**	**-3.4**	**16.4**	**-15.6**	**-13.3**	**13.1**
	RF3	**102.1**	**-44.8**	**-10.7**	**41.6**	**8.3**	**8.3**
Discectomy	**RF1**	**-42.0**	**63.7**	**-5.9**	**5.4**	**-7.9**	**5.1**
	RF2	**5.8**	**-4.8**	**28.3**	**-27.9**	**-27.8**	**28.2**
	RF3	**96.0**	**-120.2**	**7.1**	**-0.4**	**4.8**	**-2.4**
RtCVJt	**RF1**	**-36.5**	**65.1**	**-19.4**	**18.1**	**-83.1**	**78.1**
	RF2	**16.8**	**-13.5**	**33.4**	**-29.5**	**-14.5**	**18.9**
	RF3	**80.4**	**-94.8**	**85.5**	**-74.0**	**7.8**	**-2.9**
RtCTJt	**RF1**	**-36.5**	**65.1**	**-19.4**	**18.1**	**-83.1**	**78.1**
	RF2	**16.8**	**-13.5**	**33.4**	**-29.5**	**-14.5**	**18.9**
	RF3	**80.4**	**-94.8**	**85.5**	**-74.0**	**7.8**	**-2.9**
LftCVJt	**RF1**	**13.9**	**49.9**	**59.3**	**54.7**	**52.9**	**53.3**
	RF2	**-1.6**	**4.6**	**23.4**	**-12.0**	**-47.5**	**43.8**
	RF3	**60.8**	**-67.1**	**63.0**	**77.5**	**3.7**	**12.0**

Table 3 Load sharing between posterior ligaments under flexion-extension loading. Flexion = negative rotation. (ITVL/R = intertransverse ligament, left and right; SSP = supra-/inter-spinous ligament; FLAVL/R = ligamentum flavum, left and right; CAPL/R = capsular ligament, left and right, TLM = total ligament moment)

Model	***Direction***	***Rotation (degrees)***	***Total Resistive Moment at the Point of Constraint (Nmm)***	***Moment carried by ligaments Percentage of 2000Nmm, %***							***Total, TLM (%)***
				ITVL	**ITVR**	**SSP**	**FLAVL**	**FLAVR**	**CAPL**	**CAPR**	
Intact	Flexion	-0.55	2164	5.9	6.2	0	3.7	4.2	0	0	***19.9***
	Extension	0.62	-1983	0	0	0	0	0	0	0	***0***
Discectomy	Flexion	-1.20	2439	12.9	13.7	0	8.0	9.3	0	0	***43.9***
	Extension	1.55	-2677	0	0	0	0	0	3.3	11.7	***15.0***
RtCVJt	Flexion	-1.52	2382	16.2	17.6	0	10.1	11.8	2.2	0	***57.9***
	Extension	1.92	-2706	0	0	0	0	0	12.3	33.6	***45.9***
RtCTJt	Flexion	-1.52	2382	16.2	17.6	0	10.1	11.8	2.2	0	***57.9***
	Extension	1.92	-2706	0	0	0	0	0	12.3	33.6	***45.9***
LftCVJt	Flexion	-1.77	1812	19.0	20.3	0	11.8	13.7	31.9	3.3	***99.9***
	Extension	2.06	-2543	0	0	0	0	0	42.1	56.7	***98.8***

Table 4 Load sharing between posterior ligaments under left and right lateral bending. Right lateral bending = negative rotation. (ITVL/R = intertransverse ligament, left and right; SSP = supra-/inter-spinous ligament; FLAVL/R = ligamentum flavum, left and right; CAPL/R = capsular ligament, left and right, TLM = total ligament moment)

Model	***Direction***	***Rotation (degrees)***	***Total Resistive Moment at the Point of Constraint (Nmm)***	***Moment carried by ligaments Percentage of 2000Nmm, %***							***Total, TLM (%)***
				ITVL	**ITVR**	**SSP**	**FLAVL**	**FLAVR**	**CAPL**	**CAPR**	
Intact	Right	-0.38	2183	2.2	0	0	0.1	0	0	0	***2.3***
	Left	0.36	-2158	0	1.8	0	0	0.2	0	0	***2.0***
Discectomy	Right	-0.73	2329	4.4	0	0	0.3	0	0	0	***4.7***
	Left	0.74	-2320	0	3.8	0	0	0.4	0	0	***4.2***
RtCVJt	Right	-1.30	2426	7.9	0	0	0.5	0	0	0	***8.4***
	Left	1.31	-2375	0	6.8	0	0	0.7	0	0	***7.5***
RtCTJt	Right	-1.30	2426	7.9	0	0	0.5	0	0	0	***8.4***
	Left	1.31	-2375	0	6.8	0	0	0.7	0	0	***7.5***
LftCVJt	Right	-4.99	2299	49.9	0	0	1.7	0	30.8	17.5	***99.9***
	Left	5.29	-2098	0	42.2	0	0	2.8	15.8	38.5	***99.3***

Table 5 Load sharing between posterior ligaments under left and right axial rotation. Right axial rotation = negative rotation. (ITVL/R = intertransverse ligament, left and right; SSP = supra-/inter-spinous ligament; FLAVL/R = ligamentum flavum, left and right; CAPL/R = capsular ligament, left and right, TLM = total ligament moment)

Model	***Direction***	***Rotation (degrees)***	***Total Resistive Moment at the Point of Constraint (Nmm)***	***Moment carried by ligaments Percentage of 2000Nmm, %***							***Total, TLM (%)***
				ITVL	**ITVR**	**SSP**	**FLAVL**	**FLAVR**	**CAPL**	**CAPR**	
Intact	Right	-0.34	1998	0	0	0	0	0	0	0	***0***
	Left	0.32	-1986	0.2	0.2	0	0	0	0	0	***0.4***
Discectomy	Right	-0.73	1991	0	0	0	0	0	0	0	***0***
	Left	0.72	-1990	0.5	0.5	0	0	0	0	0	***1.0***
RtCVJt	Right	-1.41	2035	0	0	0	0	0	0	3.2	***3.2***
	Left	1.41	-2030	1.2	1.0	0	0	0	2.2	0	***4.4***
RtCTJt	Right	-1.41	2035	0	0	0	0	0	0	3.2	***3.2***
	Left	1.41	-2030	1.2	1.0	0	0	0	2.2	0	***4.4***
LftCVJt	Right	-1.86	1952	0	0	0	0	0	18.3	80.1	***98.4***
	Left	1.82	-2007	1.5	1.5	0	0	0	88.6	6.7	***98.3***

Figure(s)

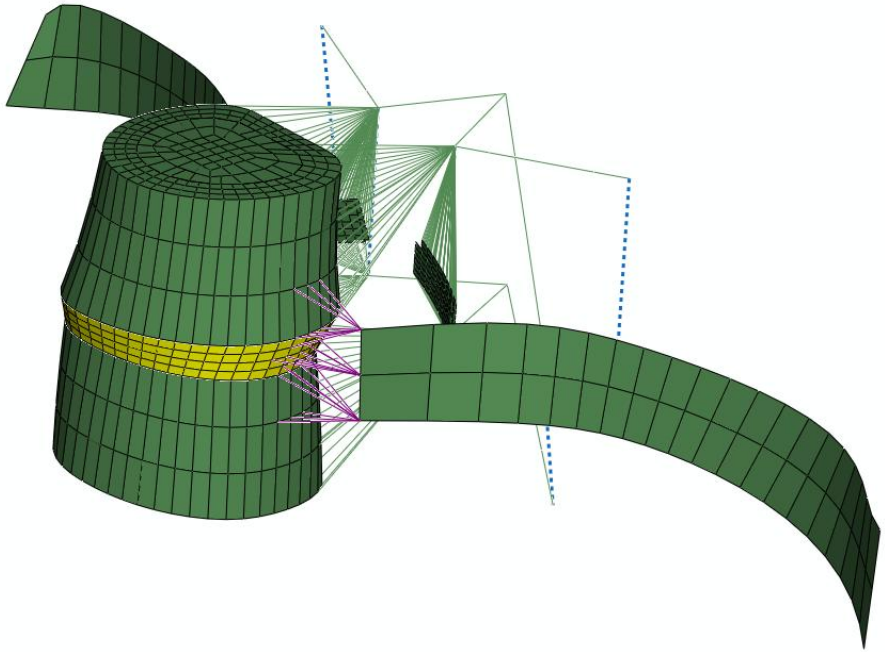

A

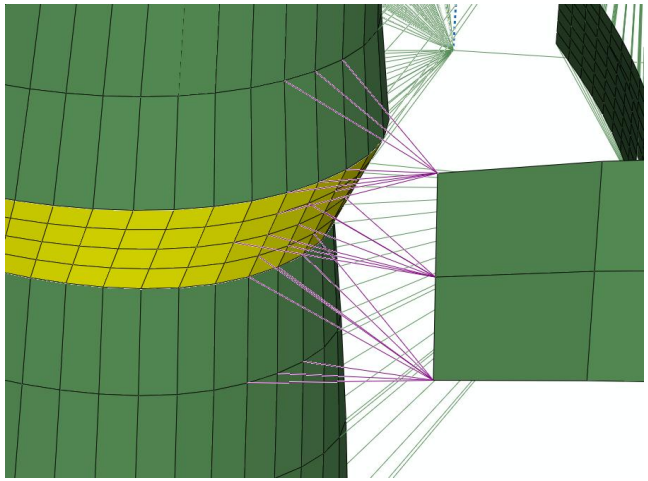

B

Figure 1

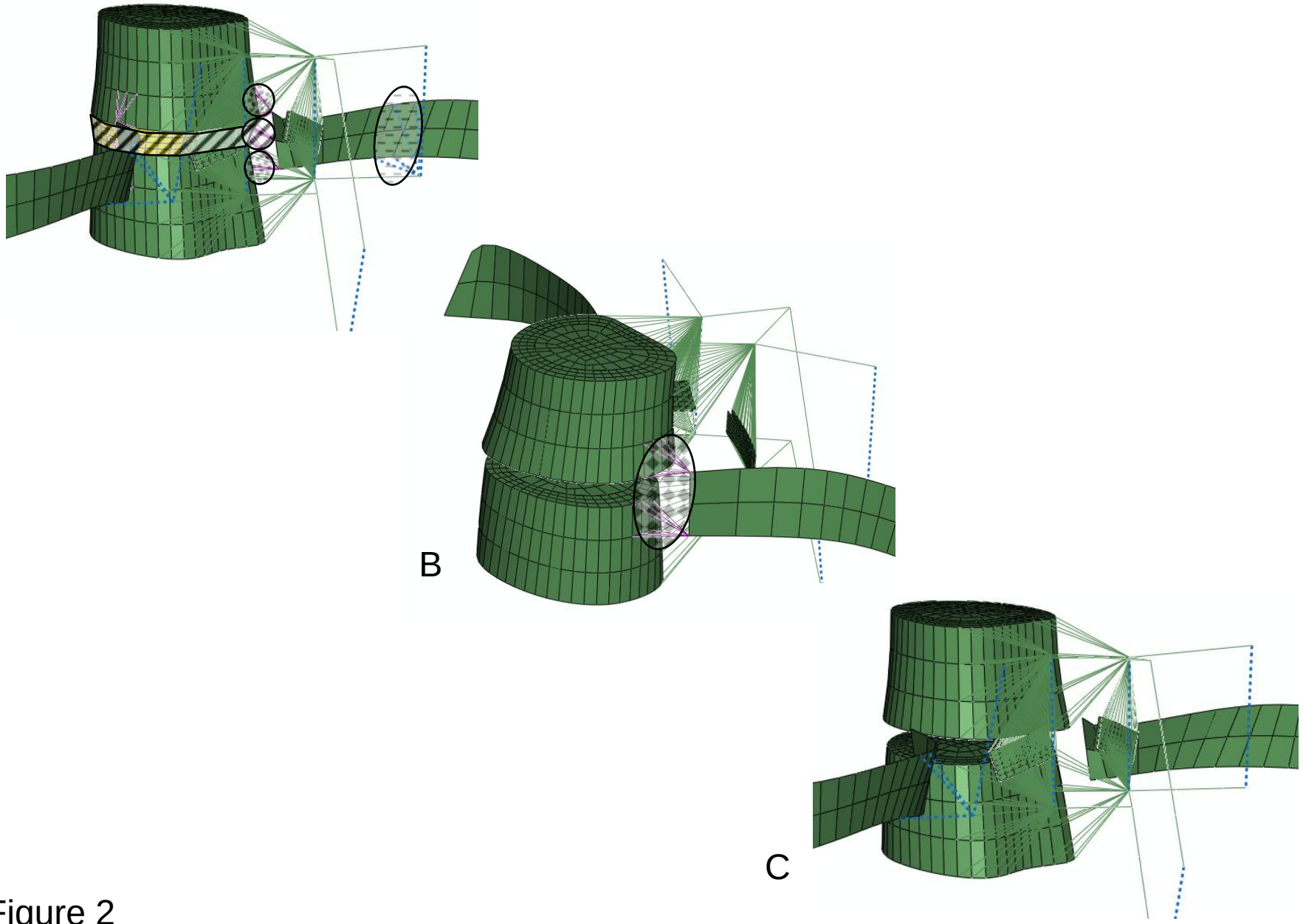

Figure 2

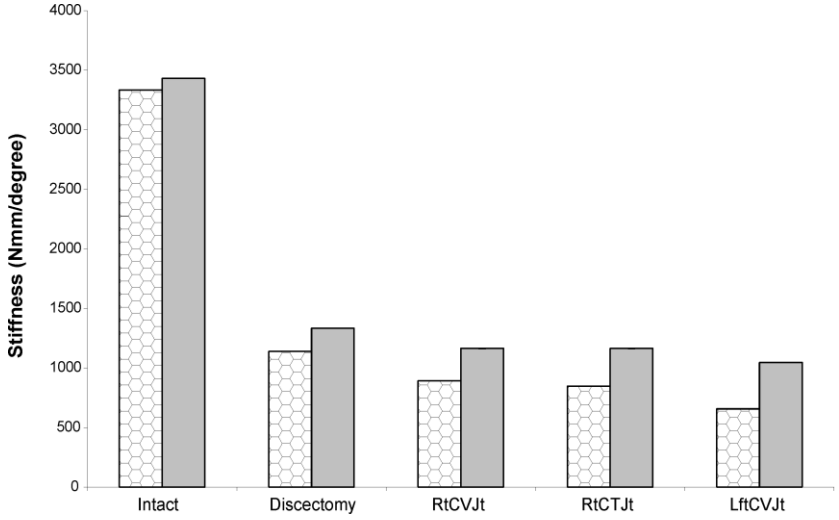
Stiffness (Nmm/degree)
4000
3500
3000
2500
2000
1500
1000
500
0
Intact
Discectomy
RtCVJt
RtCTJt
LftCVJt

A

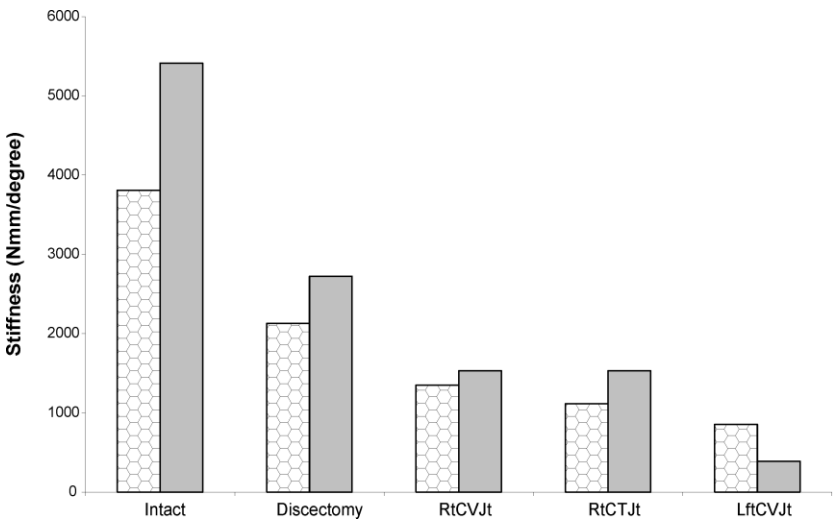
Stiffness (Nmm/degree)
6000
5000
4000
3000
2000
1000
0
Intact
Discectomy
RtCVJt
RtCTJt
LftCVJt

B

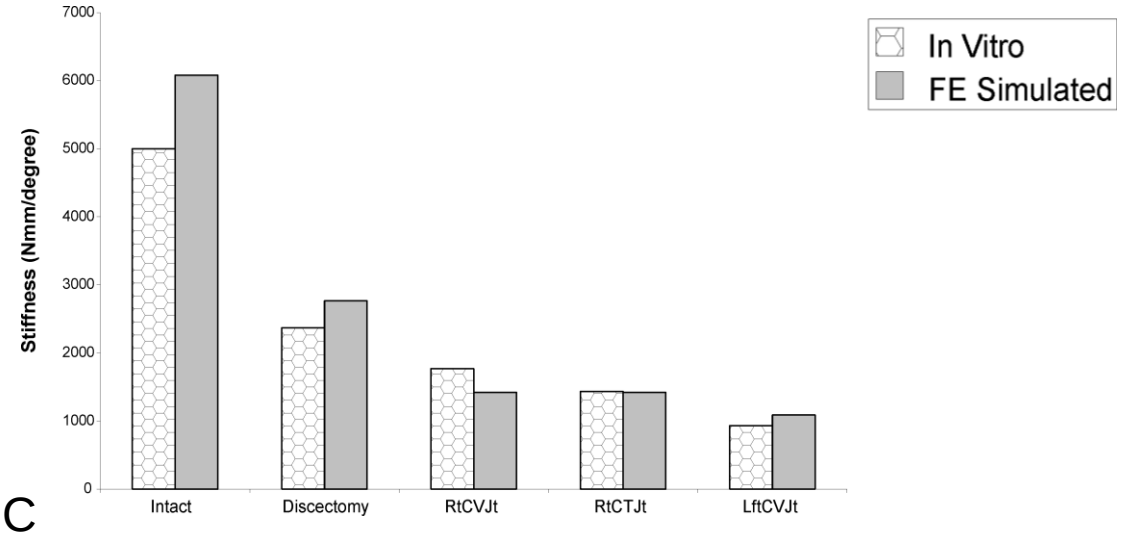
Stiffness (Nmm/degree)
7000
6000
5000
4000
3000
2000
1000
0
Intact
Discectomy
RtCVJt
RtCTJt
LftCVJt
In Vitro
FE Simulated

C

Figure 3

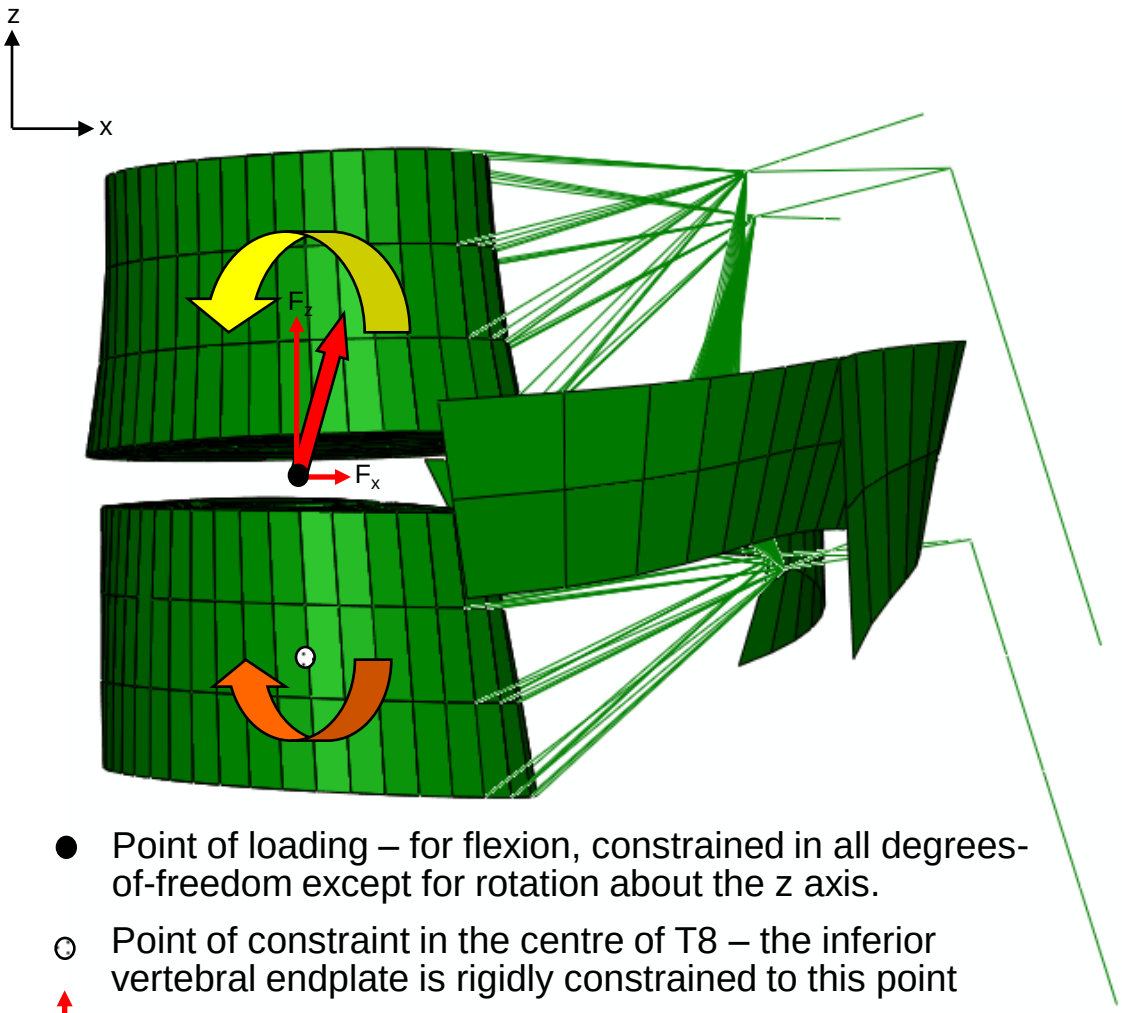

- Point of loading – for flexion, constrained in all degrees-of-freedom except for rotation about the z axis.
- Point of constraint in the centre of T8 – the inferior vertebral endplate is rigidly constrained to this point
- Reaction force components – F_x = 13.9N; F_z = 60.8
- Reaction force resultant
- Applied flexion moment at the point of loading – 2000Nmm
- Reaction moment at T8 – 1812Nmm

Figure 4